Journal of Modern Optics

ISSN: 0950-0340 (Print) 1362-3044 (Online) Journal homepage: http://www.tandfonline.com/loi/tmop20

Demonstration of chirped-pulse compression with an object-image-grating self-tiling grating compressor

Zhaoyang Li, Tao Wang, Guang Xu, Xiaoping Ouyang, Dawei Li, Hui Wei, Jianwei Yu, Lei Chen & Yaping Dai

To cite this article: Zhaoyang Li, Tao Wang, Guang Xu, Xiaoping Ouyang, Dawei Li, Hui Wei, Jianwei Yu, Lei Chen & Yaping Dai (2014) Demonstration of chirped-pulse compression with an object-image-grating self-tiling grating compressor, Journal of Modern Optics, 61:6, 495-499, DOI: 10.1080/09500340.2014.897390

To link to this article: http://dx.doi.org/10.1080/09500340.2014.897390

Journal of Modern Optics, 2014
Vol. 61, No. 6, 495–499, http://dx.doi.org/10.1080/09500340.2014.897390

Taylor & Francis
Taylor & Francis Group

Demonstration of chirped-pulse compression with an object-image-grating self-tiling grating compressor

Zhaoyang Li[a,b,c*], Tao Wang[a,c], Guang Xu[c,d], Xiaoping Ouyang[c,d], Dawei Li[c,d], Hui Wei[c,d], Jianwei Yu[c,d], Lei Chen[b] and Yaping Dai[a,c,e]

[a]*Shanghai Institute of Laser Plasma, China Academy of Engineering Physics, Shanghai, China;* [b]*School of Electronic and Optical Engineering, Nanjing University of Science and Technology, Nanjing, China;* [c]*National Laboratory for High Power Laser Physics, Shanghai, China;* [d]*Shanghai Institute of Optics and Fine Mechanics, Chinese Academy of Sciences, Shanghai, China;* [e]*Research Center of Laser Fusion, China Academy of Engineering Physics, Mianyang, China*

(*Received 11 January 2014; accepted 12 February 2014*)

The capability of chirped-pulse compression and beam focusing of an object-image-grating self-tiling grating compressor is demonstrated in an optical parametric chirped-pulse amplification laser for the first time. Probe lasers for tiling error adjustments, which are generally required by the traditional tiled-grating compressor, are not needed in our demonstration any more. With the aid of the double-sized effective optical aperture of the second grating in the compressor, a 490 fs near-transform-limit pulse duration and a 90 μm near-diffraction-limit focal spot are obtained, synchronously, which are very close to the ones achieved by a non-tiled grating compressor with equal-sized individual gratings.

Keywords: chirped pulse amplification; grating compressor; tiled grating

1. Introduction

Ultra-intense laser, such as petawatt (10^{15} W) and exawatt (10^{18}W), is a hot spot recently [1–5]. The generation of femtosecond multi-petawatt lasers, such as ELI-beamlines [6] and Vulcan 10-petawatt [7], and picosecond petawatt lasers, such as Omega-EP [8], Gekko MII [9], PETAL [10], and SGII-PW [11], is enabled by the chirped-pulse amplification (CPA) technique [12,13]. The temporal compression of chirped long-pulses is a key process for a CPA system to obtain ultra-short pulses. The parallel grating pair method proposed by E. B. Treacy usually is used to introduce a large amount of negative chirp to reconstruct an unchirped original short pulse [14]. A large pulse-width compression ratio in a treacy compressor requires a several-meter long slant distance. The angular dispersion at the first grating and the long slant distance within the grating pair will lead to a pulse spatial profile laterally broadening at the second grating. Therefore, a sufficient large grating is required. Moreover, in a high-energy ultra-short laser, the beam aperture needs to be expanded to a sub-meter level to avoid laser-induced damages of gratings [15], which further challenges the manufacture of large gratings. Recently, a near 2 m grating was needed by the 10 petawatt design of the ELI-beamlines in Czech [6], which is much larger than the available largest grating of 0.96 m. In future, this problem of grating-size-limit will continue to challenge huge ultra-intense laser facilities such as ELI (200 petawatt) [1].

The object-image-grating self-tiling (OIGST) method presented by our group is a new way to enlarge the effective optical size of a grating by tiling it with a mirror [16]. The mirror is placed perpendicular to the grating, and thereby the image of the grating will be produced behind the mirror surface. The image grating and the object grating will form a two-segment tiled grating and double the effective optical size of the original individual grating. In an OIGST tiled grating, there are only three types of tiling errors between two segment gratings: “tilt” (rotation around grating lines), “rot” (in-plane rotation), and “shift” (in-plane transfer perpendicular to grating lines), and the other three types of tiling errors: line-density variation, “tip” (rotation around the grating vector), and “piston” (transfer perpendicular to the grating surface) that challenge the traditional grating tiling method [17,18] are eliminated adequately with the aid of the object-image relationship. Thereby, it becomes very convenient to achieve and maintain the near-ideal tiled grating condition only by observing the far-field diffraction focal spot distribution of an arbitrary wavelength arbitrary incident angle monochromatic probe laser passing the seam of the tiled grating. Recently, the potential problem of the higher requirements for adjustment accuracy and maintaining stability existing in the OIGST

*Corresponding author. Email: zzyylee@gmail.com

method has been solved, as well [19]. However, up to the present, this efficient and simple method has not been used in a CPA laser to verify its usability. In this paper, we report the temporal (chirped-pulse compression) and spatial (beam focusing) demonstration of an OIGST grating compressor in an optical parametric chirped-pulse amplification (OPCPA) laser at our laboratory. This work is the feasibility research of introducing OIGST into our future10-petawatt laser facility.

2. Demonstration and result

The demonstration laser system, as shown in Figure 1, is a standard OPCPA system which consists of an oscillator, a stretcher, an amplifier, and a compressor. A 250 fs (FWHM) short pulse at 1053 nm center wavelength with a 6.5 nm (FWHM) bandwidth from a Nd:glass oscillator is deeply chirped to 3.3 ns by an eight-pass Offner-grating stretcher with a 18.6 nm spectrum window and a 400 mm 1740 g/mm gold-coated grating. After a two-stage LBO and BBO-based optical parametric amplification, the single-pulse energy is amplified from 0.5 nJ to 85 mJ. Then the amplified chirped-pulses are injected into an OIGST grating compressor and dechirped to high intense short pulses.

The top view of the OIGST grating compressor is shown in Figure 1. The compressor consists of two 1740 g/mm multilayer dielectric (MLD) gratings (G1 & G2) and two roof mirrors (RM1 & RM2). G1 is a 100 mm (width) × 200 mm (height) individual grating. G2 is an OIGST tiled grating consisting of a 200 mm (width) × 200 mm (height) individual grating and a 100 mm (width) × 200 mm (height) aluminum-coated imaging mirror. The imaging mirror doubles the effective optical size (width) of the grating from 200 to 400 mm by tiling the object grating (solid line) with its image grating (dash line), and the spatial width of the tiling seam is 3 mm. An 8 mm diameter chirped-pulse beam is incident on G1 at 70° by an injecting mirror, and the spectrum-based spatial laterally broadening beam arrives on G2 with a slant propagation distance of 2.43 m (1053 nm center wavelength). Accordingly, the shorter wavelength components are diffracted by the object grating to complete the first pass. The longer wavelength components are reflected and then diffracted by the imaging mirror and the object grating, respectively, and experience a second imaging mirror reflection to complete the first pass. The actual optical paths (solid line) for longer wavelength components are exactly equal to the virtual paths (dash line) diffracted by the image grating directly. The two roof mirrors retro-reflect the chirped-pulse beam passing the parallel grating pair (G1 & G2) for four-pass and separate the input and output beams in the height direction. The final compression beam is divided by a splitter into two beams: one is focused by a short-length (f = 150 mm) transmission lens to examine the beam focusing quality; and the other one is delivered into a single-shot second-harmonic autocorrelator to check the pulse compression capability.

Before the experiment, as shown in Figure 1, the surface and grating lines of the object grating in G2 are aligned to be parallel to those of G1, and then tiling errors ("tilt", "rot", and "shift") of the image grating with respect to the object grating in G2 are adjusted relatively by driving the imaging mirror based on a precision mechanics holder with two orthogonal mirror surface rotation motions (10 μrad sensitivity) and one mirror surface normal direction translation motion (around 50 nm

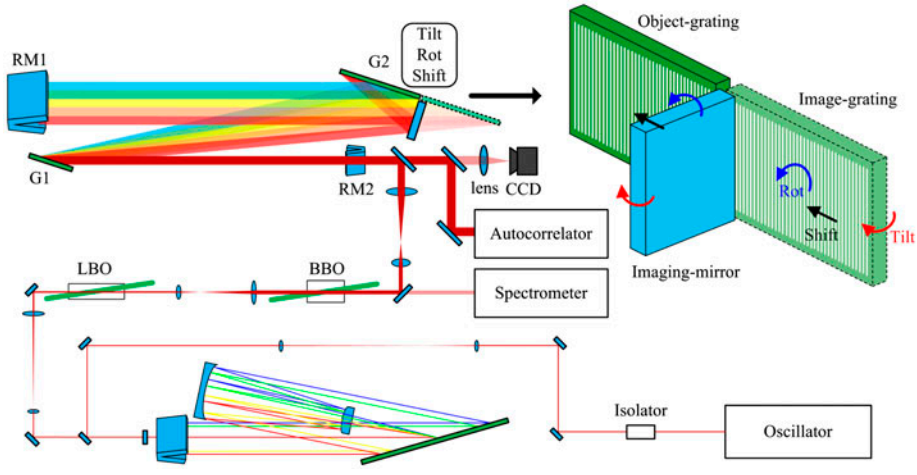

Figure 1. Schematic view of the optical system for the chirped-pulse compression demonstration. The four-pass grating compressor consists of a single grating (G1), an OIGST tiled grating (G2), and two roof mirrors (RM1 & RM2). Three types of tiling errors ("tilt", "rot", and "shift") exist within the OIGST tiled grating (G2). (The color version of this figure is included in the online version of the journal.)

resolution). Generally, in a traditional tiled grating compressor, one or several probe lasers are needed to remove six types of tiling errors [20]. However, in our compressor, no probe laser is needed, and tiling errors of the OIGST tiled grating can be removed by directly observing the far-field focal spot distribution of the main laser in the CCD camera. Figure 2(*a*) shows the far-field focal spot distribution before the image grating (the imaging mirror) adjustment. The right and the left focal spots are formed by the object and the image gratings, respectively. The horizontal and the vertical offsets of the left focal spot relative to the right one are caused by "tilt" and "rot" of the image grating with respect to the fixed object grating. Therefore, we just need to drive the two rotation motions of the imaging mirror to remove "tilt" and "rot" of the image grating by eliminating the two-direction focal spot offsets, and a 90 μm single focal spot is obtained as shown in Figure 2(*b*). The resolution of the offset of focal spots and accordingly the deviation angle between beams from object- and image-gratings is around 3 μm and 20 μrad, respectively, and the resolution of "tilt" and "rot" of the image grating with respect to the object grating is about 10 μrad. As introduced previously, the tiling error "shift" within a tiled grating would cause the focal spot to split symmetrically [17]. However, the obvious focal spot split phenomenon does not appear when we drive the imaging mirror in its normal direction ("shift" of the image grating). The reason is that very few spectral components near the center wavelength cover the tiling seam in the condition of a small beam diameter and a wide bandwidth. Only the focal spot from the spectral component covering the tiling seam will split with "shift" of the image grating; and the overlap of focal spots from all spectral components could avoid the appearance of this phenomenon. In this situation, the influence of "shift" of the image grating could be neglected. Hence, we just need to drive the translation motion of the imaging mirror ("shift" of the image grating) to reduce the tiling seam as small as possible to reduce spectral clipping and energy waste. In order to examine the result, a contrast experiment is carried out, we replace the OIGST tiled grating by a 400 mm (width) × 200 mm (height) individual MLD grating, and a reference focal spot captured by the CCD camera is shown in Figure 2(*c*). Figure 2(*d*) gives the horizontal direction focal spot intensity distributions of Figure 2(*b*) and 2(*c*), and the sizes of two focal spots are almost the same. The diffraction-limit profile of a 8 mm diameter top-hat beam is also given in Figure 2(*d*), and the actual focal spot size is around 1.9 × diffraction-limit of the theoretical one. The reason of capturing focal spots directly by a CCD camera without introducing a microscope is to eliminate the uncertainty of a magnification process and obtain the real size of focal spots, although the resolution is not high enough.

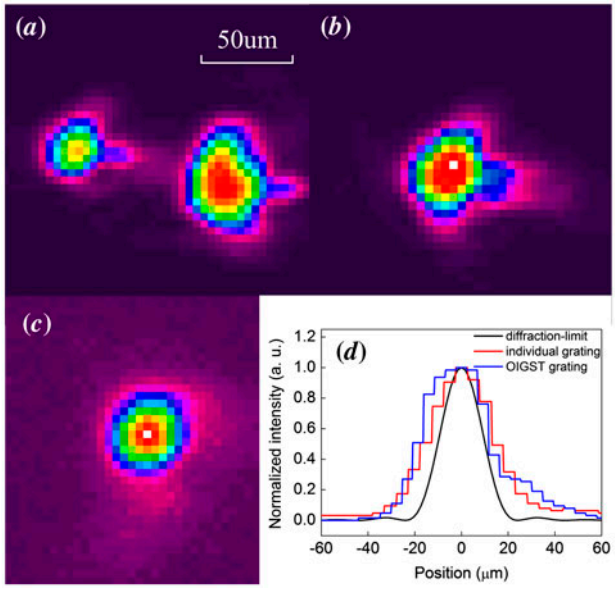

Figure 2. Far-field focal spots of the OIGST grating compressor (*a*) before and (*b*) after the tiling error adjustment. (*c*) A far-field focal spot of the non-tiled grating compressor. (*d*) Focal spot horizontal direction intensity distributions for an ideal 8 mm top-hat beam, the non-tiled grating compressor, and the OIGST grating compressor, respectively. (The color version of this figure is included in the online version of the journal).

Before measuring temporal profiles of compression pulses, we should discuss the influence of the reflection ratio of the imaging mirror, firstly, which only exists in the OIGST grating compressor. As shown in Figure 1, longer wavelength components are reflected eight times by the imaging mirror while passing the four-pass OIGST grating compressor. The reflection ratio of the aluminum-coated imaging mirror we used is about 95%. Figure 3 gives the theoretical simulation results of the non-tiled grating compressor (or the OIGST grating compressor with a 100% reflection ideal imaging mirror) and the OIGST grating compressor. In the spectrum domain, as shown in Figure 3(*a*), the dent in the middle of spectral profiles is caused by the spatial gap within the tiled grating. The intensity loss of longer wavelength components is induced by the non-ideal (95%) reflection ratio of the imaging mirror. The corresponding Fourier-transform temporal profiles are shown in Figure 3(*b*) and (*c*). The non-ideal reflection ratio of the imaging mirror reduces the peak intensity of compression pulses. Fortunately, the simulation shows the pulse duration and the temporal contrast, which are two key parameters generally concerned in ultra-high lasers, cannot be distorted obviously. In this condition, this influence can be neglected. In order to obtain the theoretical limit of compression pulses in our demonstration, the amplified spectral profile after the OPCPA and before the

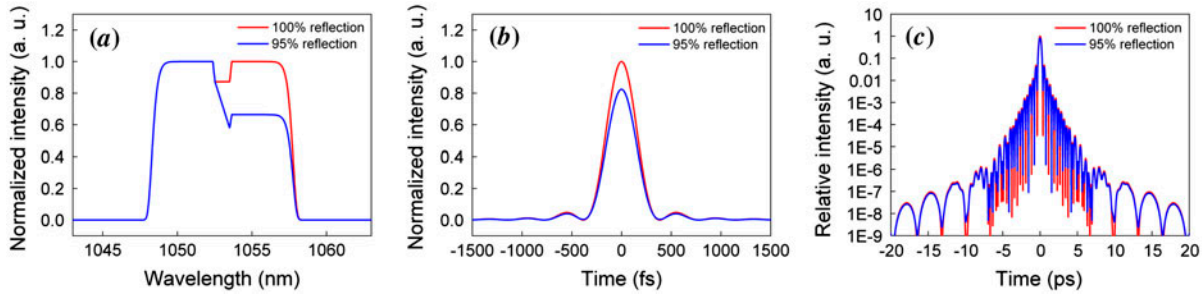

Figure 3. (*a*) Simulated spectral profiles after the OIGST grating compressor for an ideal (100% reflection) imaging mirror and an actual (95% reflection) one, respectively. Simulated (*b*) normalized and (*c*) relative Fourier-transform temporal profiles for two spectral profiles. (The color version of this figure is included in the online version of the journal.)

compressor, as shown in Figure 4(*a*), is measured. The second-order autocorrelation signal of its Fourier-transform pulse, as shown by black lines in Figure 4(*d*) and (*e*), is calculated. Figure 4(*b*) and (*c*) show streak images (time axis from left to right) of compression pulses for the non-tiled grating compressor and the OIGST grating compressor captured by the single-shot second-harmonic autocorrelator, respectively. The fine profiles are shown in Figure 4(*d*) and (*e*). According to our experiment results, pulse durations and temporal contrasts of compression pulses with two compressors meet each other very well. The pulse duration is around 490 fs (FWHM) corresponding to a 690 fs (FWHM) autocorrelation width, which is around 1.5 × Fourier-transform-limit. The dynamic range of the CCD camera in the single-shot second-harmonic autocorrelator is 33 dB; thereby, as shown in Figure 4(*e*), there is no signal in the range around 13 ps away from the pulse. Within the dynamic range of the diagnostic, the measured temporal contrast is much lower than the theoretical

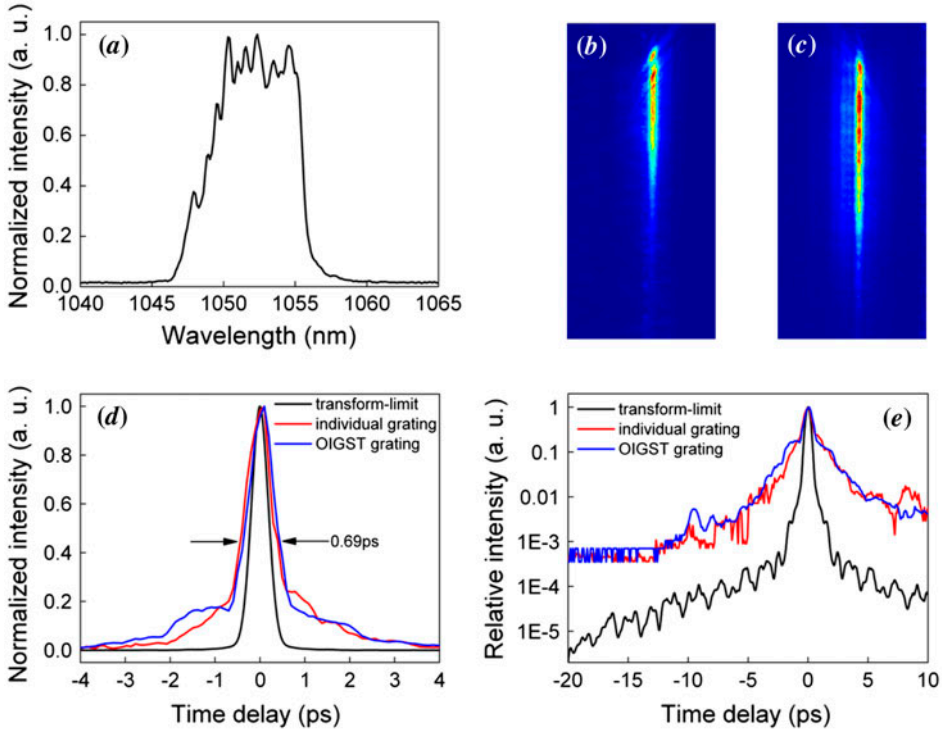

Figure 4. (*a*) A measured spectral profile before the compressor. Streak images of compression pulses for (*b*) the non-tiled grating compressor and (*c*) the OIGST grating compressor. The vertical and horizontal axes represent space and time, respectively. (*d*) Normalized and (*e*) relative second-order autocorrelation signals for the Fourier-transform pulse of the measured spectrum, the non-tiled grating compressor, and the OIGST grating compressor, respectively. (The color version of this figure is included in the online version of the journal.)

calculated one. The calculation is only based on the amplified spectral profile, and parametric fluorescence (PF) of the amplifier, high-order dispersion errors within the stretcher-compressor and spectra phase distortion caused by the optical quality of elements are not taken into account. Especially, PF is a major poor temporal contrast contributor to a pure OPCPA laser system, and similar conclusion can be found in Ref. [21]. Fortunately, PF is not relevant to grating tiling. The experiment result shows that the OIGST grating compressor has already obtained a well similar temporal compression pulse exactly like the one achieved by a large-sized non-tiled grating compressor. In this condition, we could believe the OIGST tiled grating can be used in an OPCPA or a CPA laser to enlarge the effective optical size of gratings for chirped-pulse compression. The asymmetric profile of autocorrelation signals in Figure 4(*d*) and (*e*) is caused by the non-uniform distributions of two arms of the autocorrelator in the near field, which can be found in our previous works Ref. [22] and will not be further discussed in this paper.

The efficiency of the MLD gratings, the aluminum-coated imaging mirror, and the other mirrors in our demonstration is around 97, 95, and 99.5%. The measured single pulse energy after the compressor is 55 mJ with the OIGST tiled grating, and 63 mJ with the large-sized individual grating, respectively. This energy loss can be reduced by replacing the recent imaging mirror with a new one of a higher reflection ratio, for example 99.5%. The demonstration based on broadband dielectric mirrors with a higher reflection ratio is under preparation, and the results will be reported in future.

3. Conclusion

In conclusion, we compressed a deep chirped 3.3 ns chirped-pulse to about 490 fs (1.5 × Fourier-transform-limit) and obtained a 90 μm focal spot (1.9 × diffraction-limit) by utilizing an OIGST tiled grating in a chirped-pulse grating compressor. This is the first time the OIGST method has been introduced in an OPCPA or CPA laser. Near large-sized individual grating performance is achieved, and no probe laser is required. This method is proved that can be used to solve the grating-size-limit problem existing in CPA or OPCPA lasers.

Funding

This work was supported by the National Natural Science Foundation of China [grant number 11304296], [grant number 11204330], [grant number 11204331].

References

[1] Powell, D. *Nature* **2013,** *500*, 264–265.
[2] Frolov, S.; Trunov, V.; Pestryakov, E.; Leshchenko, V. *Quantum Electron.* **2013,** *43* (5), 481–488.
[3] Hooker, C.; Tang, Y.; Chekhlov, O.; Collier, J.; Divall, E.; Ertel, K.; Hawkes, S.; Parry, B.; Rajeev, P.P. *Opt. Express* **2011,** *19* (3), 2193–2203.
[4] Xu, Y.; Guo, X.; Huang, Y.; Li, Y.; Lu, X.; Wang, C.; Liu, Y.; Wang, W.; Zhang, H.; Leng, Y.; Liang, X.; Shen, B.; Li, R.; Xu, Z. *Laser Phys. Lett.* **2013,** *10* (9), 095302-1–095302-4.
[5] Chen, Y.; Yuan, P.; Qian, L. *J. Opt.* **2011,** *13* (7), 075205-1–075205-5.
[6] Kramer, D.; Novák, J.; Rus, B. *EPJ Web Conf.* **2013,** 48 00010.
[7] Hernandez-Gomez, C.; Blake, S.P.; Chekhlov, O.; Clarke, R.J.; Dunne, A.M.; Galimberti, M.; Hancock, S.; Heathcote, R.; Holligan, P.; Lyachev, A.; Matousek, P.; Musgrave, I.O.; Neely, D.; Norreys, P.A.; Ross, I.; Tang, Y.; Winstone, T.B.; Wyborn, E.B.; Collier, J. *J. Phys. Conf. Ser.* **2010,** *244*, 032006-1–032006-4.
[8] Qiao, J.; Kalb, A.; Nguyen, T.; Bunkenburg, J.; Canning, D.; Kelly, J.H. *Opt. Lett.* **2008,** *33* (15), 1684–1686.
[9] Habara, H.; Xu, G.; Jitsuno, T.; Kodama, R.; Suzuki, K.; Sawai, K.; Kondo, K.; Miyanaga, N.; Tanaka, K.A.; Mima, K.; Rushford, M.C.; Britten, J.A.; Barty, C.P.J. *Opt. Lett.* **2010,** *35* (11), 1783–1785.
[10] Blanchot, N.; Bar, E.; Behar, G.; Bellet, C.; Bigourd, D.; Boubault, F.; Chappuis, C.; Coïc, H.; Damiens-Dupont, C.; Flour, O.; Hartmann, O.; Hilsz, L.; Hugonnot, E.; Lavastre, E.; Luce, J.; Mazataud, E.; Neauport, J.; Noailles, S.; Remy, B.; Sautarel, F.; Sautet, M.; Rouyer, C. *Opt. Express* **2010,** *18* (10), 10088–10097.
[11] Xu, G.; Wang, T.; Li, Z.; Dai, Y.; Lin, Z.; Gu, Y.; Zhu, J. *Rev. Laser Eng.* **2008,** Suppl., 1172–1175.
[12] Strickland, D.; Mourou, G. *Opt. Commun.* **1985,** *56* (3), 219–221.
[13] Maine, P.; Strickland, D.; Bado, P.; Pessot, M.; Mourou, G. *IEEE J. Quantum Elect.* **1988,** *24* (2), 398–403.
[14] Treacy, E.B. *IEEE J. Quantum Elect* **1969,** *5* (9), 454–458.
[15] Poole, P.; Trendafilov, S.; Shvets, G.; Smith, D.; Chowdhury, E. *Opt. Express* **2013,** *21* (22), 26341–26351.
[16] Li, Z.; Xu, G.; Wang, T.; Dai, Y. *Opt. Lett.* **2010,** *35* (13), 2206–2208.
[17] Zhang, T.; Yonemura, M.; Kato, Y. *Opt. Commun.* **1998,** *145*, 367–376.
[18] Cotel, A.; Castaing, M.; Pichon, P.; Le Blanc, C. *Opt. Express* **2007,** *15* (5), 2742–2752.
[19] Li, Z.; Wang, T.; Xu, G.; Li, D.; Yu, J.; Ma, W.; Zhu, J.; Chen, L.; Dai, Y. *Appl. Opt.* **2013,** *52* (4), 718–725.
[20] Hornung, M.; Bödefeld, R.; Siebold, M.; Schnepp, M.; Hein, J.; Sauerbrey, R.; Kaluza, M.C. *Appl. Opt.* **2007,** *46* (30), 7432–7435.
[21] Musgrave, I.; Shaikh, W.; Galimberti, M.; Boyle, A.; Hernandez-Gomez, C.; Lancaster, K.; Heathcote, R. *Appl. Opt.* **2010,** *49* (33), 6558–6562.
[22] Ouyang, X.; Ma, J.; Yang, L.; Tang, S.; Liu, C.; Peng, Y.; Qian, L.; Zhu, B.; Zhu, J.; Lin, Z. *Appl. Opt.* **2012,** *51* (18), 3989–3994.